Catalysis Science & Technology

PAPER

View Article Online
View Journal | View Issue



Cite this: *Catal. Sci. Technol.*, 2018, **8**, 3562

# Enhanced electrocatalytic ethanol oxidation reaction in alkaline media over Pt on a 2D $BiVO_4$-modified electrode under visible light irradiation†

Jiayue Hu,[a] Chunyang Zhai,*[a] Lixi Zeng,[b] Yukou Du [c] and Mingshan Zhu *[ab]

Received 28th April 2018,
Accepted 20th June 2018

DOI: 10.1039/c8cy00864g

rsc.li/catalysis

Bismuth vanadate ($BiVO_4$), as a typical visible-light-activated semiconductor, has attracted much attention in water oxidation. In this paper, we extend it to be a visible-light responsive support for the application of electrocatalytic ethanol oxidation reaction (EOR). Firstly, two dimensional (2D) $BiVO_4$ nanosheets were synthesized, and then worked as the support for the decoration of Pt nanoparticles. Pt nanoparticles of ultra-small size with an average diameter of 3.5 nm were well dispersed on the surface of as-synthesized 2D $BiVO_4$ nanosheets. By using the as-prepared Pt–$BiVO_4$ as a working electrode, 2.7 folds enhanced catalytic activity for the EOR were achieved under visible light irradiation compared to that under dark conditions. The synergistic effect of photocatalysis and electrocatalysis together with the 2D structure of $BiVO_4$ result in the improvement of the catalytic performance.



## 1. Introduction

Bismuth-based materials such as BiOX (X = Cl, Br, I), $Bi_2WO_6$, $Bi_2O_2CO_3$, and $BiVO_4$ have attracted the attention of researchers due to their excellent photocatalytic activity under UV and visible light irradiation, chemical stability, unique layered structures, low/non-toxicity, and abundance in nature.[1–8] Among them, $BiVO_4$ is considered to be a better photocatalytic material due to its narrow band gap (~2.4 eV) with a wide wavelength response range.[6–10] Moreover, $BiVO_4$ exhibits strong oxidation properties with chemical/photochemical stability. To date, it has been widely used in various fields of photocatalysis and photoelectrochemical tandem cells.[6–10] However, most of the above applications only focus on water oxidation, and limited efforts have been made to extend it to other areas.

On the other hand, with the overuse of petroleum energy, the worsening environmental pollution and the decreasing storage of fossil fuels on earth, it is the theme of today's world to find new clean energy sources.[11,12] Direct ethanol fuel cells (DEFCs) have aroused widespread concern of energy researchers at home and abroad due to their high energy conversion efficiency, and clean and pollution-free nature.[13–15] We have known that the catalytic performance of anode catalysts is the main factor affecting the widespread commercial application of DEFCs.[16,17] Pt and Pt-based anode catalysts have been considered as the most promising electrocatalysts for DEFCs.[18,19] However, slow kinetics of electron transfer, high cost, and being easily poisoned by intermediates (such as CO) of pure Pt have limited the commercial application of DEFCs.[20–22] Therefore, exploring a new type of high-efficiency and low-cost electrocatalyst is the main research direction.

In recent years, by using semiconductors as supports of noble metal electrocatalysts, noble metal/semiconductor hybrids have been used as efficient electrocatalysts towards alcohol oxidation reactions under light irradiation.[12,16] The optical properties of semiconductors allow them to have a strong oxidizing ability when they are excited by photo-energy under light irradiation, followed by oxidation of small organic molecules, which are adsorbed on the electrode surface, thereby resulting in enhanced catalytic activity and anti-poisoning ability.[12,16] Therefore, it is strongly desirable to explore the potential of $BiVO_4$ as a photo-activated support for depositing Pt electrocatalysts for photoelectrocatalytic oxidation of ethanol.

We all have known that two dimensional (2D) structures are the most ideal supports for the decoration of Pt nanoparticles (NPs) compared to other designed-structures or irregular shapes.[23–26] This is due to their large specific surface area, which is favorable for the dispersion of precious metal catalyst, improving the utilization of catalyst and thereby enhancing the catalytic activity. Herein, 2D $BiVO_4$ nanosheets were synthesized and then used as the support for the

[a] *School of Materials Science and Chemical Engineering, Ningbo University, Ningbo 315211, P.R. China. E-mail: mingshanzhu@yahoo.com, zhaichunyang@nbu.edu.cn*
[b] *Guangdong Key Laboratory of Environmental Pollution and Health, School of Environment, Jinan University, Guangzhou 510632, P.R. China*
[c] *College of Chemistry, Chemical Engineering and Materials Science, Soochow University, Suzhou 215123, P. R. China*

† Electronic supplementary information (ESI) available. See DOI: 10.1039/c8cy00864g

decoration of Pt NPs. It can be seen that ultra-small Pt NPs with an average diameter of 3.5 nm were well dispersed on the surface of $BiVO_4$ nanosheets. Finally, the as-prepared Pt–$BiVO_4$ electrode shows 2.7 times higher electrocatalytic performance towards the EOR with the assistance of visible light irradiation compared to that under dark conditions. The unique 2D structure and broad response in visible light of $BiVO_4$ nanosheets result in the improved catalytic performance. These outstanding photoelectrocatalytic activities indicated that the 2D $BiVO_4$ nanosheets can be used as an ideal photo-activated support for Pt electrocatalysts in DEFCs.

# 2. Experimental section

### 2.1. Materials

Bismuth nitrate pentahydrate ($Bi(NO_3)_3{\cdot}5H_2O$), ammonium vanadate ($NH_4VO_3$), sodium dodecylbenzenesulfonate ($C_{18}H_{29}NaO_3S$, SDBS), sodium hydroxide (NaOH), chloroplatinic acid hexahydrate ($H_2PtCl_6{\cdot}6H_2O$), ethanol ($CH_3CH_2OH$), potassium hydroxide (KOH), and all other chemicals were purchased from Sinopharm Chemical Reagent Co., Ltd. without purification before use.

### 2.2. Synthesis of $BiVO_4$ nanosheets

The $BiVO_4$ nanosheets were prepared by a hydrothermal method.[27] In a typical process, 5.0 mmol (2.45 g) of $Bi(NH_3)_3{\cdot}5H_2O$ was dissolved in 10.0 mL of 4.0 mol $L^{-1}$ $HNO_3$ solution, while 5.0 mmol (0.58 g) of $NH_4VO_3$ was dissolved in 10.0 mL of 2.0 mol $L^{-1}$ NaOH solution. Then, 0.72 mmol (0.25 g) of SDBS was added to both of the above solutions. After stirring for 0.5 h, the two solutions were mixed into one solution. The pH value of the mixed solution was adjusted to 7.0 by 2.0 mol $L^{-1}$ NaOH solution, and the mixture solution was further stirred for 0.5 h. This precursor solution was poured into a Teflon-lined autoclave until 80% of the volume of the autoclave was occupied. The autoclave was heated at 200 °C for 1.5 h. After the autoclave was cooled to room temperature, the yellow precipitate was separated by high-speed centrifugation, washed with distilled water and ethanol several times, and then dried at 80 °C overnight.

### 2.3. Preparation of Pt–$BiVO_4$ nanocomposites and the Pt–$BiVO_4$-modified electrode

The Pt deposited $BiVO_4$ nanocomposites were obtained by a photo-reduction method. The preparation process is as follows: 40 mg $BiVO_4$ and 0.7 ml $H_2PtCl_6$ ($3.8 \times 10^{-2}$ M) were added to 10 mL water including 20 vol% methanol in a 30 mL glass tube. Then, the tube was sealed and purged with Ar gas for 30 min before initiating the irradiation. The as-prepared sample was irradiated with Xe light under magnetic stirring for 1 h. The precipitates were collected by centrifugation, washed with water and ethanol thoroughly, and then dried at 60 °C overnight. The loading amount of Pt decorated on the surface of $BiVO_4$ nanosheets is 10 wt%.

Pt–$BiVO_4$ coated onto an L-type glassy carbon electrode (GCE, 3 mm in diameter) was synthesized as follows: 0.5, 1, 2, and 4 mg Pt–$BiVO_4$ powders were dispersed in 1 mL water–ethanol mixtures ($V_{water}:V_{ethanol}$ = 1 : 1) and 20 μL Nafion (5%, DuPond, USA) under ultrasonication for 1 h. After that, 5 μL of above suspension was deposited onto a pre-polished GCE surface and dried at room temperature, resulting in different mass amounts of the Pt–$BiVO_4$ modified electrode.

### 2.4. Photoelectrochemical measurements

The photoelectrochemical measurements were carried out in a quartz beaker *via* a CHI 660E electrochemical workstation (Shanghai Chenhua Instrumental Co., Ltd., China) with a three electrode system, wherein the Pt–$BiVO_4$ electrode acted as a working electrode and saturated calomel electrode (SCE) and Pt wires acted as reference and counter electrodes, respectively. Cyclic voltammograms (CVs) of the Pt–$BiVO_4$ electrode were monitored in 1.0 M $CH_3CH_2OH$ + 1.0 M KOH solution in the range of −0.7 to 0.2 V (*vs.* SCE). The chronoamperometry (CA) and chronopotentiometry (CP) of the Pt–$BiVO_4$ electrode under dark conditions and visible light illumination in 1.0 M $CH_3CH_2OH$ + 1.0 M KOH solution were conducted at a potential of −0.3 V and 50 μA, respectively. Linear sweep voltammograms (LSVs) of the Pt–$BiVO_4$ electrode were investigated in 1.0 M $CH_3CH_2OH$ + 1.0 M KOH solution in the range of −0.7 to −0.3 V (*vs.* SCE). Photocurrent response measurements of the Pt–$BiVO_4$ electrode were carried out in 1.0 M $CH_3CH_2OH$ + 1.0 M KOH solution at a potential of −0.3 V. Electrochemical impedance spectroscopy (EIS) was carried out by using 1.0 M $CH_3CH_2OH$ + 1.0 M KOH solution. The EIS spectra were recorded under an AC perturbation signal of 5.0 mV over the frequency range from 100 kHz to 0.1 Hz at a potential of −0.4 V (*vs.* SCE).

The working electrodes were irradiated by using a Xe arc lamp (150 W) equipped with a UV cut-off filter (>420 nm) for visible light photoelectrochemical experiment.

### 2.5. Characterization

The morphology and structure of the products were analyzed using a scanning electron microscope (SEM, S-4700), transmission electron microscope (TEM, TecnaiG220) and HAADF-STEM-EDX (JEM-3000F, operated at 300 kV). And the crystal structures of the as-prepared samples were measured *via* X-ray diffraction (XRD, PANalytical X' Pert Pro MRD). UV-vis diffuse reflectance spectra (DRS, UV-VIS-NIR Shimadzu UV3150, Japan) were recorded to study the optical properties of the samples. X-ray photoelectron spectroscopy (XPS) performed on an ESCALab220i-XL electron spectrometer was employed to study the compositions. Fourier transform infrared (FTIR) spectra were acquired with a Shimadzu FTIR-8900 spectrometer. The Brunauer–Emmett–Teller (BET) surface area was estimated using AsiQMVoTV000000-7 model instruments to analyze the products.

## 3. Results and discussion

Firstly, the morphology and component of the as-prepared $BiVO_4$ were characterized by TEM, SEM and EDX spectroscopy. Fig. 1A clearly shows the as-prepared $BiVO_4$ with a 2D nanosheet structure, and the size of the $BiVO_4$ nanosheets ranges from 100 to 600 nm. This structure provides a great place for the attachment of Pt NPs. Secondly, to further demonstrate the components of $BiVO_4$, the HAADF-STEM image with the corresponding EDX elemental mapping images of the as-prepared $BiVO_4$ nanosheets were obtained (Fig. 1B–E). The results clearly show 2D sheet-like $BiVO_4$ with different components O, V and Bi elements in the as-detected samples. The SEM images of the as-prepared samples were provided. Fig. S1† shows the 2D nanosheet structure of $BiVO_4$. After Pt nanoparticles were deposited on the surface of $BiVO_4$, some particles can be observed on $BiVO_4$. To confirm the components of the as-prepared samples, the EDX spectra of $BiVO_4$ and Pt–$BiVO_4$ are shown in Fig. S2.† It can be seen that all elements of $BiVO_4$ and Pt–$BiVO_4$ were successfully determined. In addition, the elemental composition of $BiVO_4$ and Pt–$BiVO_4$ is summarized in Table S1,† and the weight amount of Pt is *ca.* 11%, which is consistent with the theoretical amount of Pt (10 wt%) in our preparation process.

In order to visually observe the size and the distribution of Pt NPs on $BiVO_4$ nanosheets, the TEM images with different scanning magnifications of Pt–$BiVO_4$ were examined (Fig. 2 and Fig. S3†). From Fig. 2A, abundant Pt NPs were uniformly distributed on the surface of $BiVO_4$ nanosheets. This phenomenon shows that Pt NPs are well dispersed on the surface of 2D $BiVO_4$ nanosheets, confirming the advantage of 2D nanosheets. Moreover, as can be seen from Fig. 2B and the size distribution (Fig. S3†), Pt NPs were uniformly deposited on the surface of $BiVO_4$ nanosheets and the average diameter of Pt NPs was calculated to be 3.5 nm (Fig. S3B†).

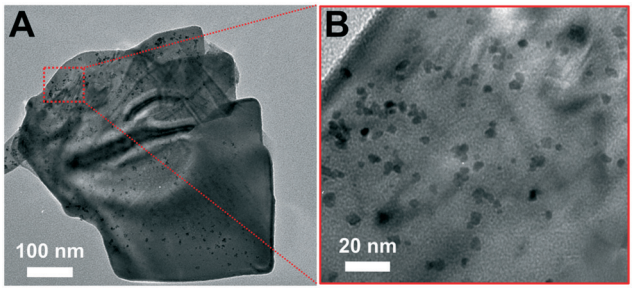


**Fig. 2** Low (A) and high (B) magnification TEM images of Pt–$BiVO_4$ nanocomposites.

In addition, XPS has been employed to investigate the chemical composition and interaction between Pt and $BiVO_4$ in the Pt–$BiVO_4$ composites, as shown in Fig. 3. Firstly, in the $BiVO_4$ sample, two peaks, Bi $4f_{7/2}$ and Bi $4f_{5/2}$, with binding energies at 159.3 and 164.8 eV are observed in Fig. 3A.[28,29] For the Pt–$BiVO_4$ sample, the corresponding peaks of Bi $4f_{7/2}$ and Bi $4f_{5/2}$ shift to 160.4 and 166.2 eV, respectively. Besides that, two signals at 517.4 and 524.5 eV in Fig. 3B are ascribed to V $2p_{3/2}$ and V $2p_{1/2}$, respectively, which can be assigned to the $V^{5+}$ ion of $BiVO_4$.[30–32] In the Pt–$BiVO_4$ sample, similar to Bi, the peaks of V 2p also have a shift and are located at 518.6 and 524.7 eV for V $2p_{3/2}$ and V $2p_{1/2}$, respectively. These

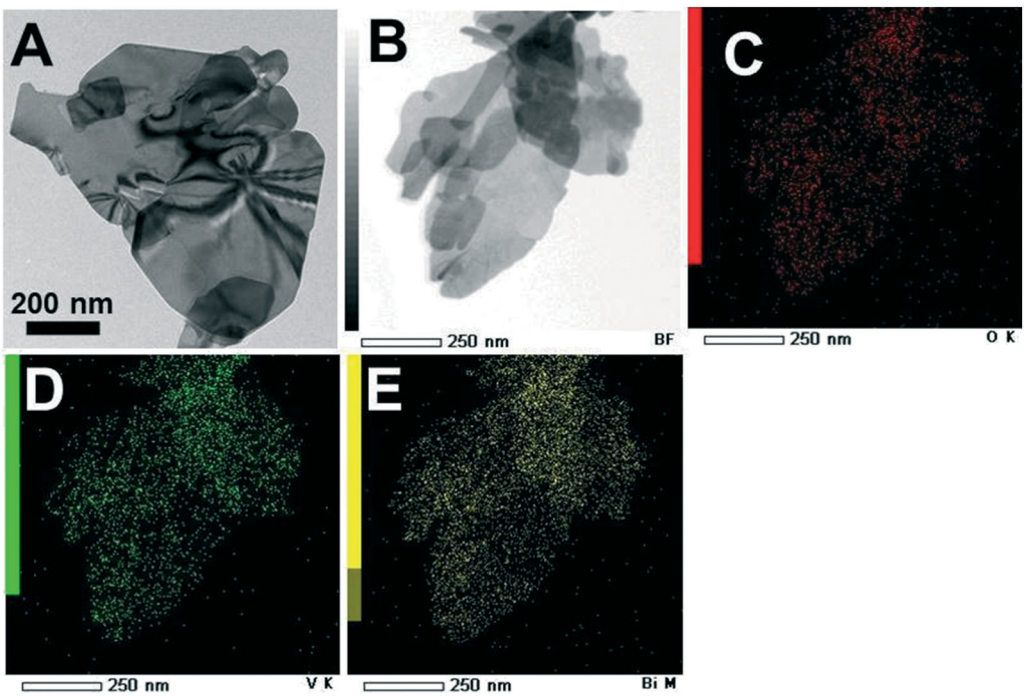


**Fig. 1** TEM image (A), HAADF-STEM image (B), and the corresponding EDX elemental mapping images of O (C), V (D), and Bi (E) elements of $BiVO_4$ nanosheets.

 

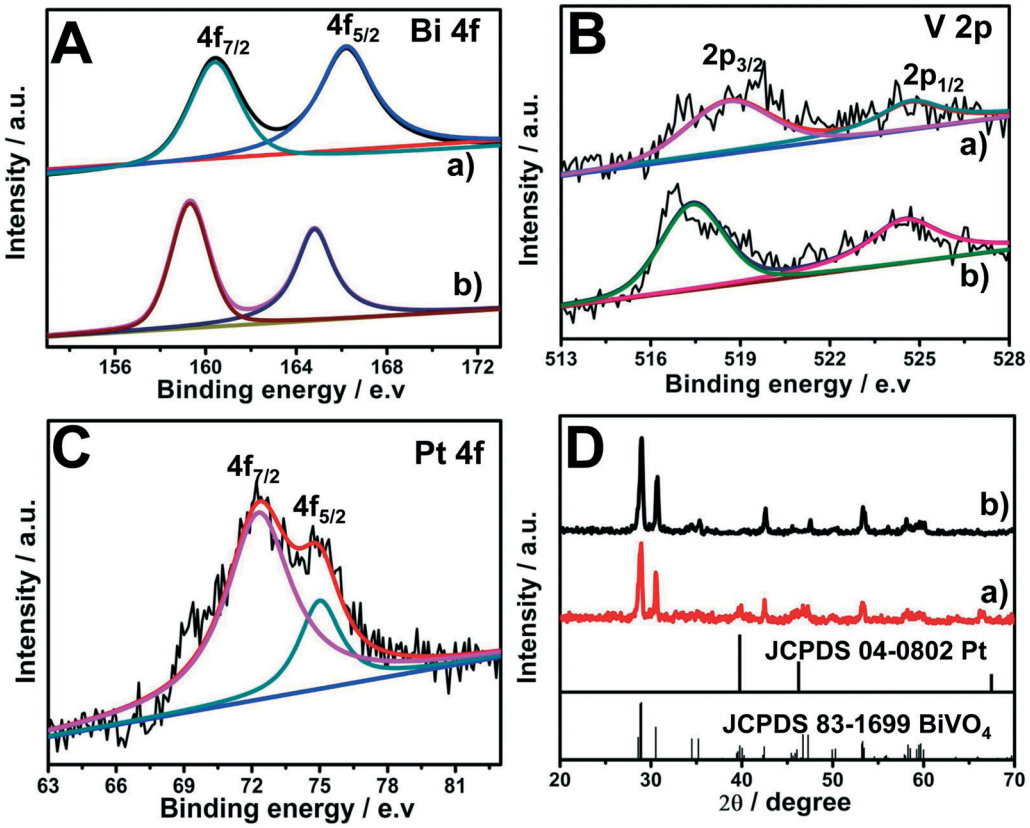


Fig. 3 XPS spectra of Bi 4f (A), V 2p (B), and Pt 4f (C) of Pt–$BiVO_4$ (a) and $BiVO_4$ (b). (D) XRD patterns of Pt–$BiVO_4$ (a) and $BiVO_4$ (b).

shifts came from the hybridization of Pt, in which the surface electrons of $BiVO_4$ are transferred to Pt.[33] Lastly, as shown in Fig. 3C, the binding energies of 71.5 and 75.2 eV correspond to Pt $4f_{7/2}$ and Pt $4f_{5/2}$, respectively.[34,35] This result indicates the successful formation of metallic Pt NPs in the $BiVO_4$ species.

To further analyze the components of $BiVO_4$ and Pt–$BiVO_4$, the XRD patterns of the as-prepared samples were also studied. As shown in Fig. 3D, all diffraction peaks in the XRD pattern of $BiVO_4$ can be readily indexed to the specific crystal planes of the $BiVO_4$ phase (JCPDS No. 83-1699).[36] This shows that well-crystallized $BiVO_4$ is obtained under the as-synthesized conditions. In addition, the weak peaks at about 39.9°, 46.5° and 67.6° correspond to the characteristic refraction of Pt, which are assigned to the diffraction of the (111), (200) and (220) planes of Pt (JCPDS No. 04-0802), respectively.[37,38] According to the Debye–Scherrer equation ($D = k\gamma/B\cos\theta$, $D$: crystal diameter, $k$: Scherrer constant, $B$: width at half maximum of the diffraction peak, $\theta$: angle of deviation, $\gamma$: X-ray wavelength), the particle size ($D$) of the Pt nanoparticles is *ca.* 3.9 nm, which is consistent with the results of TEM (3.5 nm). Moreover, the FT-IR spectra of the as-synthesized samples were detected, as shown in Fig. S4.† For $BiVO_4$, a very strong absorption band at 756 $cm^{-1}$ with a shoulder at 818 $cm^{-1}$ (V–O) was detected, which was assigned to the V–O covalent bond,[37] further confirming the formation of $BiVO_4$. After Pt nanoparticles were deposited on the surface of $BiVO_4$ nanosheets, the FT-IR spectra did not show significant changes, suggesting that the introduced Pt did not cause changes in the $BiVO_4$ structure.

Fig. 4 shows the UV-vis diffuse reflectance spectra of the $BiVO_4$ and Pt–$BiVO_4$ samples. It's found that typical absorption edges around 520 nm were observed in both samples, which corresponded to the intrinsic adsorption of $BiVO_4$. Moreover, in the Pt–$BiVO_4$ sample, a tail absorption band was detected in the visible region because of the black color of metallic Pt. The basic optical properties of the $BiVO_4$ semiconductor indicate that the as-prepared samples have

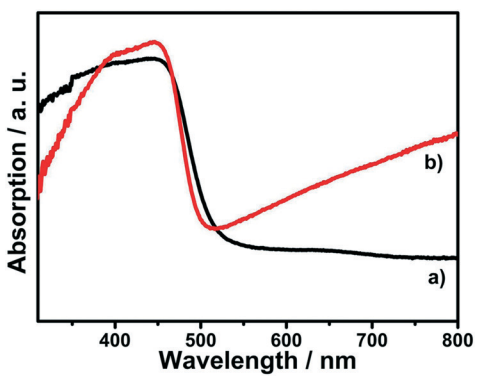


Fig. 4 UV-vis diffuse reflectance spectra of $BiVO_4$ (a) and Pt–$BiVO_4$ (b) products.

potential as visible-light-activated electrocatalysts for the electrooxidation of ethanol.[39,40]

Before evaluating the catalytic activity of the EOR, the electrochemical surface area (ECSA) of the electrode was investigated, as shown in Fig. S5.† The ECSA of Pt–$BiVO_4$ was calculated by using the equation ECSA = $Q_H/0.21{\cdot}M$, ($Q_H$: the amount of electron transfer (mC $cm^{-2}$), $M$: the amount of Pt on the electrode surface (mg $cm^{-2}$), and 0.21 (mC $cm^{-2}$) is the Pt crystalline activity surface area transfer coefficient). From Fig. S5,† the ECSA was detected to be 1.3 $m^2$ $g^{-1}$ for the Pt–$BiVO_4$ electrode under dark conditions. We also used BET to detect the surface areas of $BiVO_4$ and Pt–$BiVO_4$. The BET data show that the surface areas of $BiVO_4$ and Pt–$BiVO_4$ are 1.7 $m^2$ $g^{-1}$ and 2.5 $m^2$ $g^{-1}$, respectively, which are slightly larger than the ESCA. Interestingly, the ECSA of Pt–$BiVO_4$ increased to 2.3 $m^2$ $g^{-1}$ when the electrode was under visible light conditions. This result indicates superior charge–storage properties under visible light irradiation for the Pt–$BiVO_4$ electrode.[41]

To evaluate the catalytic performance of the as-prepared samples, the activities of Pt–$BiVO_4$ with different concentrations for the catalytic oxidation of ethanol are shown in Fig. 5. The CV measurements of Pt–$BiVO_4$ and Pt NPs were carried out in 1.0 M $CH_3CH_2OH$ + 1.0 M KOH solution under dark conditions and visible light irradiation, as shown in Fig. 5A. Firstly, in the range of −0.7–0.2 V, two peaks were detected with forward (*ca.* −0.30 V) and backward (*ca.* −0.35 V) peaks. Generally, the forward peak current density was used to evaluate the performance of EOR. Under dark conditions, the forward peak current densities were detected to be 591.3 and 608.2 mA $mg_{Pt}^{-1}$ for Pt–$BiVO_4$ and Pt NP electrodes, respectively. However, for Pt–$BiVO_4$, the peak current density is increased to 1555 mA $mg_{Pt}^{-1}$ when it was under visible light conditions. This phenomenon clearly shows that visible light promotes the electrocatalytic activity of the Pt–$BiVO_4$ in the EOR. We also summarize recent reports on electrocatalytic oxidation of ethanol by using Pt-based electrocatalysts within the last two years in Table S2.† The data show our as-prepared electrodes with superior electrocatalytic performance with the assistance of visible light irradiation. Moreover, Fig. 5B visually shows that the best electro-oxidation activity is 1555 mA $mg_{Pt}^{-1}$ at a catalyst concentration of 2 mg $mL^{-1}$ under visible light irradiation, which is much higher than electro-oxidation activities of 694, 1434, and 679 mA $mg_{Pt}^{-1}$ for 0.5, 1, and 4 mg $mL^{-1}$ under visible light irradiation, respectively. The optimum concentration for the catalyst is the concentration of 2 mg $mL^{-1}$, which is better for dispersion on the glassy carbon electrode.

To further study the PEC properties of the Pt–$BiVO_4$ catalyst, linear sweep voltammetry (LSV) of the Pt–$BiVO_4$ nanocomposites toward ethanol oxidation under dark and visible light irradiation have been performed. As shown in Fig. 6A, at a given potential of −0.25 V, the current density of the Pt–$BiVO_4$ electrode was 949.4 mA $mg_{Pt}^{-1}$ for the EOR under visible light illumination, which was *ca.* 1.9 times higher than that of Pt–$BiVO_4$ without visible light illumination (500.8 mA $mg_{Pt}^{-1}$). Additionally, the onset potential of Pt–$BiVO_4$ under visible light illumination is more negative compared to that under dark conditions, indicating the better ethanol oxidation capability.[42] The photocurrent responses of Pt–$BiVO_4$ and $BiVO_4$ were measured by on/off irradiation of visible light every 30 s in 1.0 M $CH_3CH_2OH$ +1.0 M KOH solution at −0.3 V. As can be seen in Fig. 6B, the current density of the Pt–$BiVO_4$ electrode is always higher than the $BiVO_4$ electrode, indicating the better photoelectric properties of the Pt–$BiVO_4$ nanocomposites.[43] Moreover, the response photocurrent of Pt–$BiVO_4$ with an intensity of *ca.* 0.71 mA $cm^{-2}$ upon visible light irradiation is 1.5 times higher than that when visible light irradiation is switched off (0.47 mA $cm^{-2}$).

In addition, the long-term stability of catalysts is critical for fuel cell applications. Chronoamperometric (CA) profiles were obtained by applying a potential to the electrode in 1.0 M $CH_3CH_2OH$ + 1.0 M KOH solution. From Fig. 7A, the Pt–$BiVO_4$ electrode showed an initial rapid decrease in current, which may be attributed to the accumulation of adsorbed species on the catalyst surfaces, followed by a subsequent slow current decrease.[44] In addition, it can be seen that the Pt–$BiVO_4$ catalyst with visible light irradiation had a much

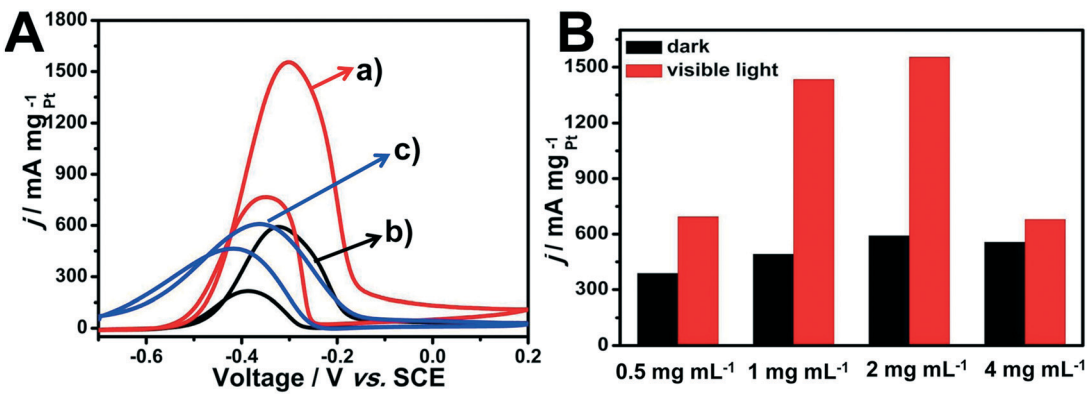


Fig. 5 A: The 20th CV of Pt–$BiVO_4$ (a and b) and Pt NPs (c) in 1.0 M $CH_3CH_2OH$ + 1.0 M KOH solution under visible light irradiation (a) and dark conditions (b). B: The histogram of activities of the Pt–$BiVO_4$ electrode with different concentrations for the catalytic oxidation of ethanol under visible light irradiation and dark conditions.

 

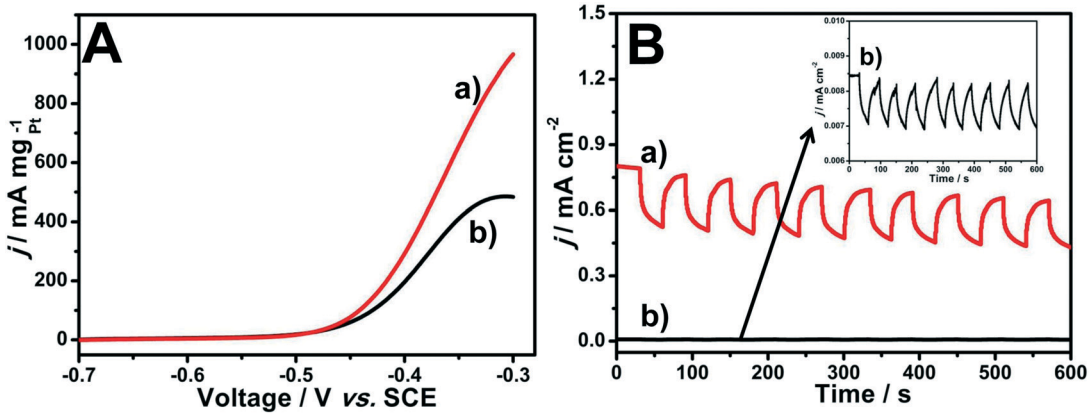


**Fig. 6** A: LSVs of the Pt–$BiVO_4$ electrode under visible light irradiation (a) and dark conditions (b) in 1.0 M $CH_3CH_2OH$ +1.0 M KOH solution. B: Photocurrent responses of Pt–$BiVO_4$ (a) and $BiVO_4$ (b) electrodes in 1.0 M $CH_3CH_2OH$ + 1.0 M KOH solution at −0.3 V. The illumination was interrupted every 30 s.

higher initial current than the Pt–$BiVO_4$ catalyst under dark conditions. More importantly, the Pt–$BiVO_4$ catalyst maintained higher currents within 2000 s of the test under visible light illumination conditions than that without light illumination. The retained oxidation current density of Pt–$BiVO_4$ for the EOR under visible light illumination after 2000 s was 6.0 mA $mg_{Pt}^{-1}$, which was 2.3 times higher than that under dark conditions (2.6 mA $mg_{Pt}^{-1}$).

Fig. 7B shows the chronopotentiometric (CP) curves of the Pt–$BiVO_4$ catalyst with and without visible light irradiation. Firstly, there is a gradual increase of electrode potential at first and then an instantaneous leap to a much higher potential. Due to the deep poisoning of the Pt–$BiVO_4$ electrode, the ethanol oxidation reaction cannot continue, and the potential must jump to a higher potential. The antipoisoning ability of catalysts can be evaluated by the time at which the electrode potential jumps to a higher potential. The sustained time values for the Pt–$BiVO_4$ electrode under visible light and dark conditions are 1015 and 365 s, respectively. Compared to dark conditions, the antipoisoning ability of the as-prepared Pt–$BiVO_4$ electrode is 2.8 fold under visible light illumination, suggesting the better stability of the electrode under visible light irradiation.

Electrochemical impedance spectroscopy (EIS) is powerful evidence to assess charge transfer resistances of electrode materials. Fig. 8A shows the Nyquist plots of the Pt–$BiVO_4$ electrode in 1.0 M $CH_3CH_2OH$ + 1.0 M KOH solution under visible light irradiation and dark conditions. It's easy to find that the diameter of the semicircle arc of the Pt–$BiVO_4$ electrode under visible light irradiation was smaller than that under dark conditions. A smaller diameter of the semicircular arc generally means a faster interface charge transfer rate. In order to visually show the charge-transfer resistance parameter, the EIS spectra were fitted with the equivalent circuits (Fig. 8B), where $R_{ct}$ is associated with the charge-transfer resistance at the electrode/solution interface, and $Q$ represents the electrode double-layer capacitance formed at the electrode/solution interface. We can find that the $R_{ct}$ of Pt–$BiVO_4$ for the EOR under visible light irradiation is 2099 Ω, which is smaller than that of the working electrode under dark conditions (4772 Ω). The above result indicates the effective interfacial charge transport and smaller resistance upon visible light illumination.

To study the photoelectrocatalytic process of the ethanol oxidation reaction, the EIS spectra of the Pt–$BiVO_4$ modified electrode at different potential ranges under visible light irradiation

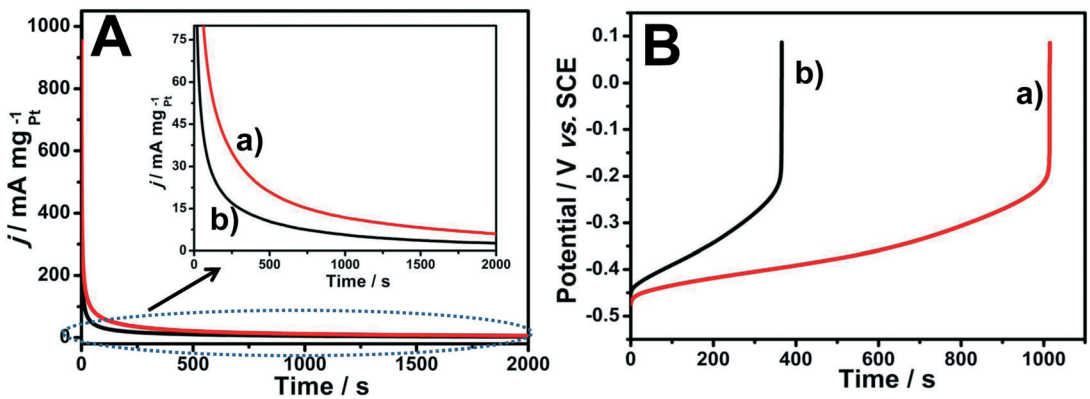


**Fig. 7** Chronoamperometric curves at −0.3 V (A) and chronopotentiometric curves at 50 μA (B) of the Pt–$BiVO_4$ electrode under visible light irradiation (a) and dark conditions (b) in 1.0 M $CH_3CH_2OH$ + 1.0 M KOH solution.

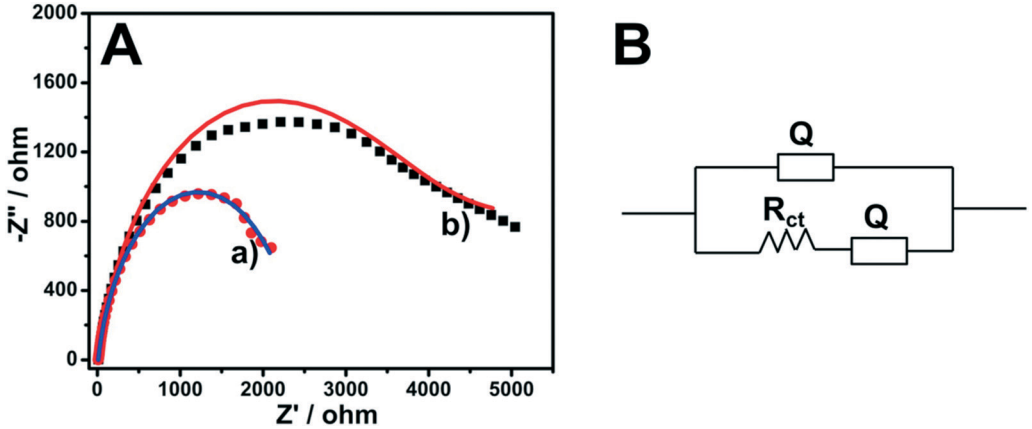


Fig. 8 A: Nyquist plots of the Pt–$BiVO_4$ electrode under visible light irradiation (a) and dark conditions (b) in 1.0 M $CH_3CH_2OH$ + 1.0 M KOH solution at −0.4 V. B: Equivalent circuit was used for simulating the impedance spectrum of the Pt–$BiVO_4$ electrode under visible light irradiation and dark conditions.

and dark conditions were investigated, as shown in Fig. 9. Firstly, under a low potential range, the diameter of the semicircle arc decreases from −0.55 V to −0.4 V both under visible light irradiation and dark conditions. This is because intermediate species, which are generated during the ethanol oxidation reaction, are removed at higher potentials, resulting in a smaller diameter of the semicircle arc.[43,45] When the potential continually increases from −0.4 to −0.25 V, owing to intermediate species poisoning at the oxidation potential, the diameter of the semicircle arc is increased. At the applied potential of −0.25 V, the arcs reversed to the second quadrant. This is due to the recovery of catalytic active sites by the removal of intermediate species from the electrode at the ethanol oxidation potential. When the potential further increased from −0.25 V to −0.1 V, the semicircle arcs returned gradually to a large diameter, because the intermediate species returned back and the Pt surface was oxidized at such a high potential.[43,45] Similar to the electrode under visible light irradiation, the Pt–$BiVO_4$ electrode shows similar tendencies while displaying much larger diameters of semicircle arcs under dark conditions. These results indicate effective interfacial charge transport upon light photo-irradiation of Pt–$BiVO_4$ in the ethanol oxidation reaction process.

To further confirm the photo-enhanced electrocatalytic oxidation activity of Pt–$BiVO_4$, the different scan rates on ethanol oxidation of the Pt–$BiVO_4$ electrode under visible light and dark conditions were investigated. As shown in Fig. 10A and C, the forward ethanol electro-oxidation peak

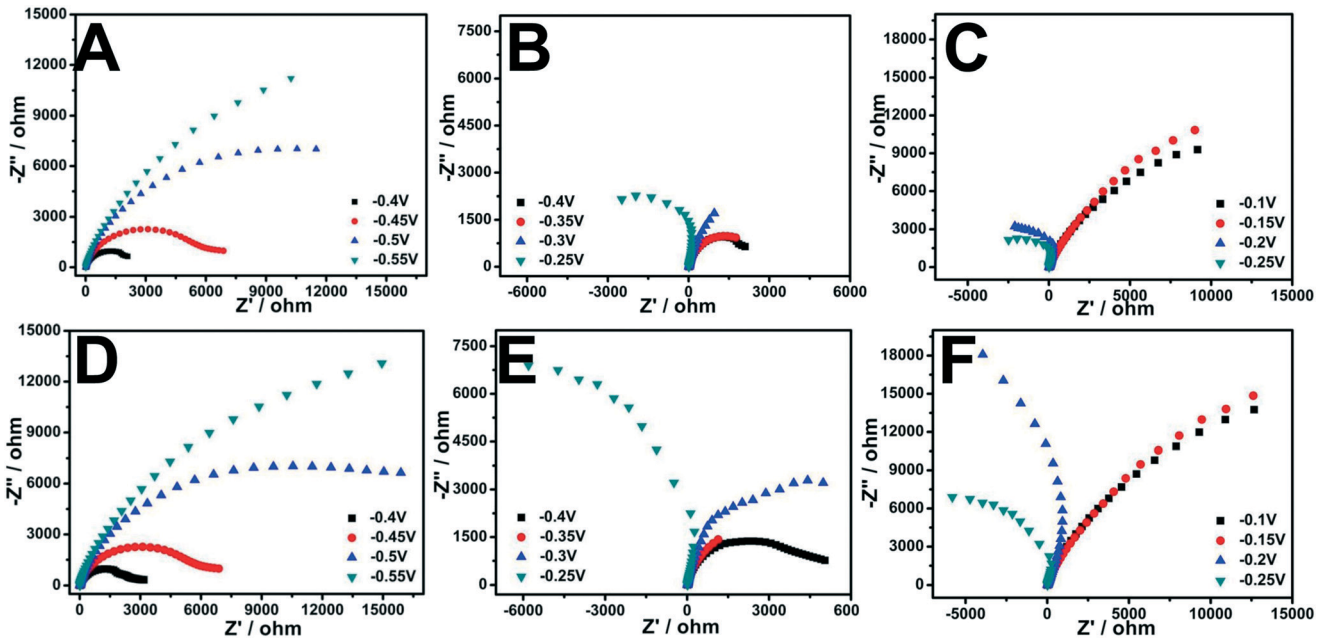


Fig. 9 EIS spectra of the Pt–$BiVO_4$ electrode in 1.0 M $CH_3CH_2OH$ + 1.0 M KOH solution at different potentials under visible light irradiation (A–C) and dark conditions (D–F).

 

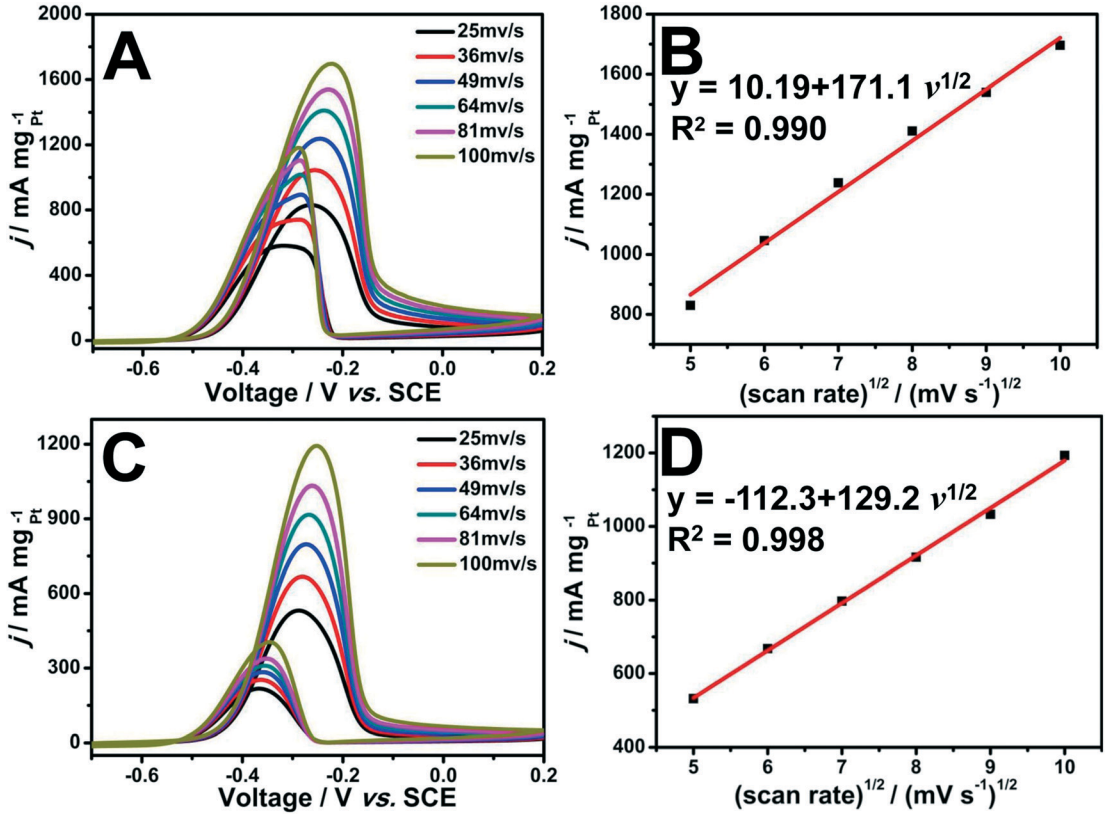


**Fig. 10** CVs of the Pt–$BiVO_4$ electrode at different scan rates under visible light irradiation (A) and dark conditions (C) in 1.0 M $CH_3CH_2OH$ + 1.0 M KOH solution. The corresponding plots of the forward peak current *versus* the square root of the scan rate under visible light irradiation (B) and dark conditions (D).

current density increased with the increase of the scan rates. Additionally, from Fig. 10B and D, the forward peak current ($i_p$) shows a linear relationship with the square root of the scan rate ($v^{1/2}$), suggesting that the photo-enhanced electrocatalytic oxidation of ethanol on the Pt–$BiVO_4$ catalyst is controlled by the diffusion process.[34,46] For the purpose of investigation on the different electron-transfer kinetics of the as-synthesized samples under visible light irradiation and dark conditions, the diffusion coefficients ($D$) of the electrode under different conditions were compared by using eqn (1):

$$\frac{D_{\text{light}}}{D_{\text{dark}}} = \left[ \frac{\left( \frac{i_p}{v^{1/2}} \right)_{\text{light}}}{\left( \frac{i_p}{v^{1/2}} \right)_{\text{dark}}} \right]^2 \quad (1)$$

The value of the ratio of diffusion coefficients ($D_{\text{light}}/D_{\text{dark}}$) is calculated to be 1.9. This result indicated that the electron transfer kinetics of the Pt–$BiVO_4$ catalyst is promoted by visible light irradiation, which results in better photo-enhanced electrocatalytic ethanol oxidation performance.[38]

Based on the above investigations, when 2D $BiVO_4$ was used as a support for the decoration of ultra-small Pt NPs, the activities and stabilities of the electrochemical properties of Pt–$BiVO_4$ were significantly enhanced under visible light irradiation. The photo-enhanced electrocatalytic EOR mechanism of Pt–$BiVO_4$ is proposed and shown in Scheme 1. Firstly, the 2D nanosheet-like $BiVO_4$ provides an ideal substrate for depositing Pt NPs, and these Pt NPs act as electrocatalysts. The ethanol molecules would be adsorbed on the surface of the electrocatalyst, and then they would be oxidized.[35] Secondly, when the electrode was under visible light irradiation, $BiVO_4$ was easily excited owing to its broad optical absorption in the visible light region. After $BiVO_4$ was

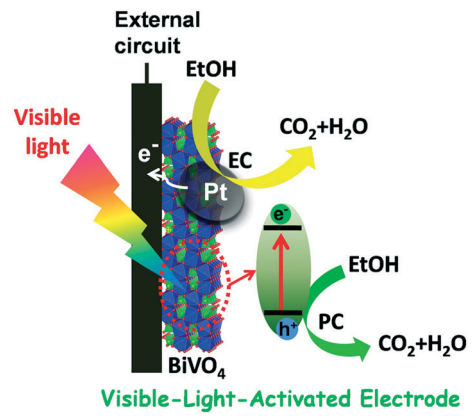


**Scheme 1** Scheme of the electrocatalytic (EC) and photocatalytic (PC) EOR on the Pt–$BiVO_4$ electrode under visible light irradiation.

excited, electrons and holes were generated in the conduction band (CB) and valence band (VB), respectively. The adsorbed ethanol molecules are oxidized on the surface of the catalyst by these holes owing to the strong oxidation ability of holes.[29] Meanwhile, the corresponding electrons on the CB were transferred to the Pt and then the electrons from the EOR were transferred to the external circuit. This electron injection results in the enhancement of the current. Moreover, the intermediates (such as CO) during the EOR process would be also removed by such holes, contributing to the higher stability of the as-prepared Pt–$BiVO_4$ electrode.[29]

## 4. Conclusions

In conclusion, 2D $BiVO_4$ nanosheets were used to be the visible-light-responsive support for the decoration of Pt NPs. The 2D nanosheets allow better dispersion of ultra-small Pt NPs on the $BiVO_4$ surface. The as-prepared Pt–$BiVO_4$ composite further acted as a high-efficiency working electrode to evaluate the electrocatalytic activity of ethanol oxidation. Due to the synergistic effect of photocatalysis and electrocatalysis, the Pt–$BiVO_4$ electrode displayed much better EOR activity and stability under visible light compared to that under dark conditions. Such high separation efficiency of photogenerated carriers leads to the boosting of the performance of photoelectrocatalytic oxidation of ethanol. This feature facilitates a new avenue for the application of $BiVO_4$ in fuel cell reactions.

## Conflicts of interest

There are no conflicts to declare.

## Acknowledgements

This work was sponsored by the K.C. Wong Magna Fund in Ningbo University. The authors appreciate the National Natural Science Foundation of China (Grant 21603111, 51702173, 41522304, and 21577142).

## References

1 H. Cheng, B. Huang and Y. Dai, *Nanoscale*, 2014, **6**, 2009–2026.
2 L. Ye, Y. Su, X. Jin, H. Xie and C. Zhang, *Environ. Sci.: Nano*, 2014, **1**, 90–112.
3 L. Chen, J. He, Y. Liu, P. Chen, C. T. Au and S. F. Yin, *Chin. J. Catal.*, 2016, **37**, 780–791.
4 R. He, S. Cao, P. Zhou and J. Yu, *Chin. J. Catal.*, 2014, **35**, 989–1007.
5 A. Sivakumar, B. Murugesan, A. Loganathan and P. Sivakumar, *J. Taiwan Inst. Chem. Eng.*, 2014, **45**, 2300–2306.
6 J. H. Kim and J. S. Lee, *Energy Environ. Focus*, 2014, **3**, 339–353.
7 C. M. Suarez, S. Hernández and N. Russo, *Appl. Catal., A*, 2015, **504**, 158–170.
8 Y. H. Xu, C. J. Liu, M. J. Chen and Y. Q. Liu, *Int. J. Nanopart.*, 2011, **4**, 268–283.
9 X. Chang, T. Wang, P. Zhang, J. Zhang, A. Li and J. Gong, *J. Am. Chem. Soc.*, 2015, **137**, 8356–8359.
10 M. Zhu, Z. Sun, M. Fujitsuka and T. Majima, *Angew. Chem., Int. Ed.*, 2018, **57**, 2160–2164.
11 M. A. F. Akhairi and S. K. Kamarudin, *Int. J. Hydrogen Energy*, 2016, **41**, 4214–4228.
12 S. Sfaelou and P. Lianos, *AIMS Mater. Sci.*, 2016, **3**, 270–288.
13 A. S. Aricò, S. Srinivasan and V. Antonucci, *Fuel Cells*, 2001, **1**, 133–161.
14 C. Koenigsmann and S. S. Wong, *Energy Environ. Sci.*, 2011, **4**, 1161–1176.
15 W. Hong, C. Shang, J. Wang and E. Wang, *Energy Environ. Sci.*, 2015, **8**, 2910–2915.
16 M. Zhu, Y. Du, M. Sun and C. Zhai, *Wuji Cailiao Xuebao*, 2017, **32**, 897–903.
17 N. Kakati, J. Maiti, S. H. Lee, S. H. Jee, B. Viswanathan and Y. S. Yoon, *Chem. Rev.*, 2014, **114**, 12397–12429.
18 M. Zhu, C. Zhai, M. Sun, Y. Hu, B. Yan and Y. Du, *Appl. Catal., B*, 2017, **203**, 108–115.
19 N. Zhang, S. Guo, X. Zhu, J. Guo and X. Huang, *Chem. Mater.*, 2016, **28**, 4447–4452.
20 W. Xia, A. Mahmood, Z. Liang, R. Zou and S. Guo, *Angew. Chem., Int. Ed.*, 2016, **55**, 2650–2676.
21 Z. Yang, H. Nie, X. a. Chen, X. Chen and S. Huang, *J. Power Sources*, 2013, **236**, 238–249.
22 J. Duan, S. Chen, M. Jaroniec and S. Z. Qiao, *ACS Catal.*, 2015, **5**, 5207–5234.
23 L. Shi, G. M. Deng, W. C. Li, S. Miao, Q. N. Wang, W. P. Zhang and A. H. Lu, *Angew. Chem., Int. Ed.*, 2015, **54**, 13994–13998.
24 S. Liu, N. Tian, A. Y. Xie, J. H. Du, J. Xiao, L. Liu, H. Y. Sun, Z. Y. Cheng, Z. Y. Zhou and S. G. Sun, *J. Am. Chem. Soc.*, 2016, **138**, 5753–5756.
25 X. Pan, X. Chen and Z. Yi, *ACS Appl. Mater. Interfaces*, 2016, **8**, 10104–10108.
26 G. Liu, Y. Qiu, Z. Wang, J. Zhang, X. Chen, M. Dai, D. Jia, Y. Zhou, Z. Li and P. Hu, *ACS Appl. Mater. Interfaces*, 2017, **9**, 37750–37759.
27 W. Wang, X. Wang, C. Zhou, B. Du, J. Cai and G. Feng, *J. Phys. Chem. C*, 2017, **121**, 19104–19111.
28 H. Xu, H. Li, C. Wu, J. Chu, Y. Yan, H. Shu and Z. Gu, *J. Hazard. Mater.*, 2008, **153**, 877–884.
29 F. Chen, Q. Yang, Y. Wang, J. Zhao, D. Wang, X. Li, Z. Guo, H. Wang, Y. Deng, C. Niu and G. Zeng, *Appl. Catal., B*, 2017, **205**, 133–147.
30 C. Zhai, J. Hu, M. Sun and M. Zhu, *Appl. Surf. Sci.*, 2018, **430**, 578–584.
31 K. P. Parmar, H. J. Kang, A. Bist, P. Dua, J. S. Jang and J. S. Lee, *ChemSusChem*, 2012, **5**, 1926–1934.
32 N. K. Veldurthi, N. K. Eswar, S. A. Singh and G. Madras, *Appl. Catal., B*, 2018, **220**, 512–523.
33 J. Zhang, Y. Lu, L. Ge, C. Han, Y. Li, Y. Gao, S. Li and H. Xu, *Appl. Catal., B*, 2017, **204**, 385–393.
34 Z. Zhang, K. Liu, Z. Feng, Y. Bao and B. Dong, *Sci. Rep.*, 2016, **6**, 19221–19231.

 

35 J. Hu, M. Sun, X. Cai, C. Zhai, J. Zhang and M. Zhu, *J. Taiwan Inst. Chem. Eng.*, 2017, **80**, 231–238.
36 J. Hu, C. Zhai, C. Yu, L. Zeng, Z. Liu and M. Zhu, *J. Colloid Interface Sci.*, 2018, **524**, 195–203.
37 D. Ke, T. Peng, L. Ma, P. Cai and K. Dai, *Inorg. Chem.*, 2009, **48**, 4685–4691.
38 X. Lin, D. Xu, Y. Xi, R. Zhao, L. Zhao, M. Song, H. Zhai, G. Che and L. Chang, *Colloids Surf., A*, 2017, **513**, 117–124.
39 M. Sun, J. Hu, C. Zhai, M. Zhu and J. Pan, *Electrochim. Acta*, 2017, **245**, 863–871.
40 M. Sun, J. Hu, C. Zhai, M. Zhu and J. Pan, *ACS Appl. Mater. Interfaces*, 2017, **9**, 13223–13230.
41 C. Zhai, M. Zhu, F. Pang, D. Bin, C. Lu, M. C. Goh, P. Yang and Y. Du, *ACS Appl. Mater. Interfaces*, 2016, **8**, 5972–5980.
42 Y. Zhao, R. Li, L. Mu and C. Li, *Cryst. Growth Des.*, 2017, **17**, 2923–2928.
43 A. R. Nanakkal and L. K. Alexander, *J. Mater. Sci.*, 2017, **52**, 7997–8006.
44 Z. Guo, X. Dai, Y. Yang, Z. Zhang, S. Mi, K. Xu and Y. Li, *J. Mater. Chem. A*, 2013, **1**, 13252–13260.
45 C. Zhai, M. Sun, M. Zhu, K. Zhang and Y. Du, *Int. J. Hydrogen Energy*, 2017, **42**, 5006–5015.
46 Z. Yao, R. Yue, F. Jiang, C. Zhai, F. Ren and Y. Du, *J. Solid State Electrochem.*, 2013, **17**, 2511–2519.